Available online at www.sciencedirect.com
ScienceDirect
Composite Structures 78 (2007) 507–518
COMPOSITE STRUCTURES
www.elsevier.com/locate/compstruct

# Stability of the face layer of sandwich beams with sub-interface damage in the foam core

Vitaly Koissin [a,*], Vitaly Skvortsov [a], Andrey Shipsha [b]

[a] Department of Strength of Materials, State Marine Technical University, 198 262 St.-Petersburg, Russia
[b] Department of Aeronautical and Vehicle Engineering, Royal Institute of Technology, S-100 44, Stockholm, Sweden

Available online 27 December 2005

**Abstract**

This paper addresses the effect of local indentation/impact damage on the bearing capacity of foam core sandwich beams subjected to edgewise compression. The considered damage is in a form of through-width zone of crushed core accompanied by a residual dent in the face sheet. It is shown that such damage causes a significant reduction of compressive strength and stiffness of sandwich beams. Analytical solutions estimating the Euler's local buckling load are obtained for two typical modes of damage. These solutions are validated through experimental investigation of three sandwich configurations. The results of the analytical analysis are in agreement with the experimental data.


*Keywords:* Sandwich structure; Indentation; Low-velocity impact; Local damage; Crushed foam core; Residual dent; Local buckling; Euler's load

## 1. Introduction

With the appearance of sandwich structures, the problem of their local bucking has become entrenched in the design process, since the core layer provides a limited support for the in-plane compressed face sheet. The local buckling (wrinkling) onset in virgin sandwiches has been investigated in many studies, e.g. Ref. [1], and a number of analytical approaches have been proposed [2]. The less studied problem is related to the case of a face-core debond or local damage in the core, when the virgin core support is reduced. Under in-plane compression, the load bearing capacity can degrade significantly from that of a perfectly bonded panel. Thomson and Mouritz, Ref. [3], measured reduction of up to 50% in stiffness and 80% in strength when the damaged sandwich composite beams were loaded in edgewise compression. Effect of a sub-interface imperfection in the core on the local buckling phenomenon has been investigated by many in the past [4], though not many analytical solutions have been worked out. The proposed solutions can roughly be divided into two general groups.

The simplified approach is based on the assumption that the sub-interface imperfection constitutes a local face-core debond, Refs. [5–9]. The virgin core is usually modelled as the Winkler foundation (in this formulation the problem has first been solved by Heténi, Ref. [10]). This approach produces simple solutions but, in a general case, can with success be used only for the particular case of a manufacture debond. Furthermore, the Winkler model provides satisfactory results not for any sandwich configuration.

The more precise but rare approach includes modelling the crushed core. For example, Wadsworth et al. [11] studied the problem using the Winkler foundation with varying stiffness. The governing equation was solved using the finite-difference method, and the results were found in good agreement with the test data. The disadvantage of the reported solutions is the use of the Winkler model with varying foundation stiffness for the crushed core, since it requires a sophisticated experimental characterization [14].

* Corresponding author. Present address: Department of Metallurgy and Materials Engineering, Katholieke Universiteit Leuven, Kasteelpark Arenberg 44, B-3001 Leuven, Belgium. Fax: +32 16 32 19 90.
*E-mail address:* vitaly@kth.se (V. Koissin).

0263-8223/$ - see front matter © 2005 Elsevier Ltd. All rights reserved.
doi:10.1016/j.compstruct.2005.11.012

The present paper extends the previous work by the authors [12–15] to investigate in more detail the local buckling phenomena in sandwich beams containing a sub-interface damage in the foam core. The purpose of this study is to present analytical methods that can predict reduction in the load bearing capacity. The proposed approach yields simple analytical solutions even when accounting for the effect of the crushed core. The analytical results are compared with test data for sandwich beams indented/impacted with a rigid cylinder. The analytical estimation of the residual strength gives satisfactory predictions with an accuracy acceptable for engineering purposes.

## 2. Experimental study

Experimental study was initially conducted to investigate the physical phenomena of local damage and local buckling in sandwich beams and thus to provide essential input for the analytical modelling. The object of study were flat beams with thick rigid foam cores and thin glass-fibre (GFRP) faces; the beams' in-plane dimension was $47 \times 270$ mm. These specimens were locally indented/impacted causing local bending of the face sheet accompanying by the core crushing and then subject to an edgewise compression, as described below in detail.

### 2.1. Sandwich configurations

We used three sandwich configurations fabricated by means of vacuum infusion. The core materials were Rohacell WF51, and Divinycell H60 and H130 rigid closed-cell foams. The face laminates were quasi-isotropic GFRP sheets. The Young's moduli of the faces were measured according to ASTM D638M. The moduli, yield stresses and yield strains of the core materials were obtained from uniaxial compression tests (ASTM D1623-78). The Poisson's ratios were estimated by the laminate theory (for the faces) or taken from the core manufacturers data sheets [16,17]. The material data is listed in Table 1.

### 2.2. Indentation and impact testing of sandwich specimens

Indentation tests were conducted in an Instron universal testing machine at cross-head displacement rate of 2 mm/min. To limit the overall bending, the sandwich beams were entirely rested on a rigid plate. The load was applied through a steel cylindrical indenter of 25 mm in diameter, as shown in Figs. 1(a) and 2(left). Four specimens were used in each set of indentation magnitude; per 1.75, 2, 2.5, 3, 4, 5, 6, 8, and 10 mm.

Typical load–displacement curve sampled during the tests is shown in Fig. 3(left). Here, the path A–B corresponds to the pure elastic response of a specimen. At the point B, the onset of core crushing occurs, and the following path B–C exhibits a progressive growth of a crushed core zone. Undergoing relatively high deflection (8, 10 mm), the faces emitted popping sounds, presumably indicating microscopic failure of individual fibres in the vicinity of the contact with the indentor. Upon unloading represented with the path C–D, a residual dent was observed in the face. The maximum magnitude of this dent was measured taking the displacement from the testing machine that corresponds to zero load during 10 min (path D–E). It was observed that the residual dent was time-

Table 1
Basic mechanical properties of the sandwich constituents

| Configuration | Material | Thickness, mm | Young's modulus, MPa | Poisson's ratio | Yield strain | Yield stress, MPa |
|---|---|---|---|---|---|---|
| 1 | WF51 | 50 | 85[a] | 0.42 | 0.012[a] | 0.9[a] |
| | GFRP | 2.4 | 19,300[b] | 0.25 | 0.002[c] | 44.3[c] |
| 2 | H60 | 50 | 88[a] | 0.32 | 0.012[a] | 0.8[a] |
| | GFRP | 2.4 | 19,300[b] | 0.25 | 0.002[c] | 44.3[c] |
| 3 | H130 | 40 | 135[a] | 0.32 | 0.014[a] | 2.3[a] |
| | GFRP | 1.6 | 15,800[b] | 0.25 | 0.002[c] | 42.8[c] |

[a] Out-plane compression.
[b] In-plane tension.
[c] Conventional value, in-plane compression (ASTM D3410).

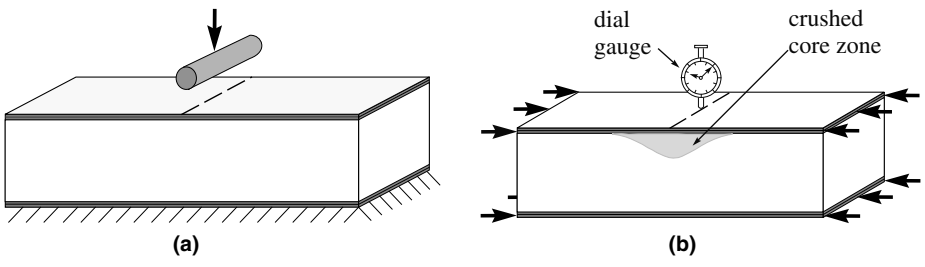


Fig. 1. A sandwich beam subject to local indentation (a) and edgewise compression (b).


Fig. 2. A sandwich beam of second configuration subject to local indentation (left) and edgewise compression (right).

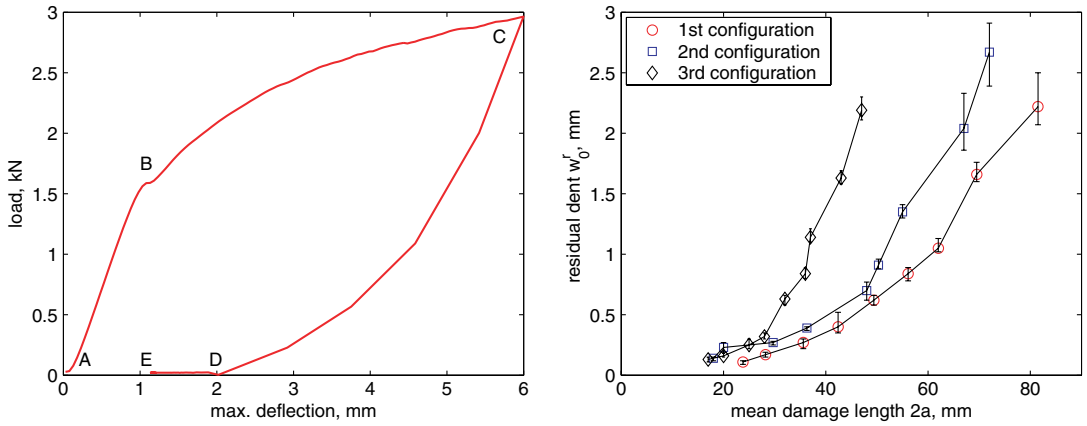


Fig. 3. Applied load vs. face deflection response for first sandwich configuration (left) and max. residual dent vs. mean damage length for indented specimens (right).

depended, and its magnitude decreased by up to 50% during the first minute. Then, the dent became stabilized, and the point E thus presented the steady magnitude of the residual dent. As it is proved below in Section 2.5, the transient instability of the residual dent should be attributed to specific properties of the crushed core.

Besides the static indentation tests, a number of specimens were subjected to localized transverse impacts. The impact tests were conducted in a drop-weight test rig with the same impactor tip and support conditions as in the quasi-static indentation tests. The total impact mass was kept of 7.8 kg, and the impact energy was varied by changing a drop height assuming the ideal free fall. Six impact energies were used; 6.6, 13.3, 20, 26.5, 33.3, and 40 J. After rebound, the impactor was captured to avoid a secondary impact of a specimen. Series of 4–5 specimens for each impact energy were tested.

### 2.3. Results of indentation and impact tests

Observation of the tested specimens revealed a limited damage (fibre delamination and matrix cracking) in the face nearby the contact area with the indenter/impactor. As has been shown in the previous study by one of the authors, Ref. [13], a such damage decreased the bending stiffness of the face only by 5% in comparison with intact laminate (for the first sandwich configuration). Thus, the damage was mainly manifested in the form of the crushed core and residual dent in the face as shown in Fig. 4(a).

Impacted specimens with H60 or H130 foam core have shown the same damage as in the static tests, and thus were not investigated further. In the specimens with WF51 foam core, the impact damage was observed as a through-width cavity surrounded by the crushed core as shown in Fig. 4(b). Nucleation of this cavity could be caused by rapid straightening of the face after the impactor rebound and related effects in the crushed core (WF-grade foams are relatively brittle even in undamaged state). The cavity was located some small distance below the face, since core cells at the interface were enriched and, thereby, strengthened by the adhesive. The cavity formation resulted in almost zero (max. 0.2 mm) magnitude of the residual dent as compared to the static indentation tests. The residual dent was measured after several hours after the impact tests moving a dial gauge over the face surface.

The crushed core zone was clearly observed during and after the tests, since it had specific appearance and color. The mean measured damage lengths, $2a$, are summarized

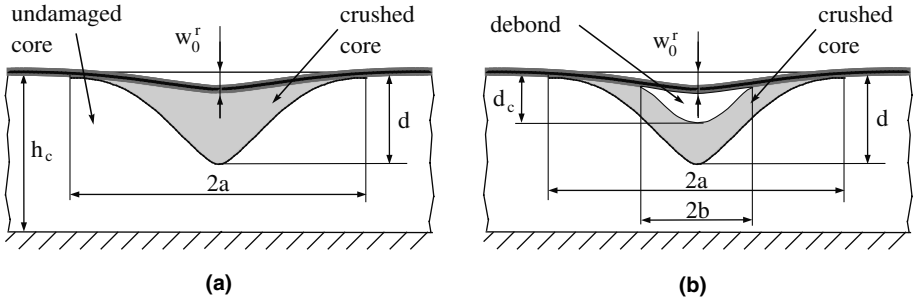


Fig. 4. Damage without (a) and with (b) face-core debond.

in Fig. 3(right) as functions of the maximum residual dent, $w_0^r$. The ratio of the damage depth, $d$, to the damage length, $2a$, was 0.05–0.14, 0.11–0.15, or 0.11–0.21 for first, second, and third sandwich configurations, respectively. The test results showed only a minor scatter, with a maximum divergence from the average values of less than 10%. In the impacted specimens with WF51 foam core, the cavity length, $2b$, was approximately 1/2 of the overall length of the core damage, $2a$. The same proportion was observed between the cavity depth, $d_c$, and the damage depth, $d$. A more detailed data for the first sandwich configuration can be obtained in Ref. [13].

### 2.4. Edgewise compression of sandwich specimens

The edgewise compression tests were performed according to ASTM C364–94; the test set-up is schematically shown in Fig. 1(b). The edges of the specimens were reinforced with tabs and milled to ensure that they were flat and parallel. The specimens were compressed between two steel plates at the cross-head displacement rate of 2 mm/min. A dial gauge was used for measuring the out-plane displacements at the centre of the residual dent as shown in Fig. 1(b). Since the in-plane stiffness of the faces was much greater than that of the core layer, the compressive stress $\sigma$ in the faces was calculated as

$$\sigma = P/2h_f b, \tag{1}$$

where $P$ is the total load sampled from the press, $h_f$ is the face thickness, and $b$ is the beam width.

The behaviour of the specimens with indent- or impact-induced damage under edgewise compression was found to be mainly depended on the magnitude of the residual face dent, $w_0^r$, and size of the core damage, $2a$. The following failure modes were observed:

*Classical wrinkling* in the manner of abrupt bifurcation leading to a complete disintegration of a sandwich structure. This failure mode was common for specimens with WF51 or H60 core having small residual dent (including all impacted specimens with WF51 core). The wrinkling wave pattern was well manifested by the foam core which remained on the detached faces.

*Face yielding* which resulted in abrupt yielding failure of the face laminate. This was exhibited by the indented specimens with H130 core having small residual dent and damage size. This face failure mainly took place near the tabs and could thus be explained by the stress concentration.

*Failure in the core* due to overall bending initiated by the local buckling in the damaged area. The indented beams with WF51 and H60 cores (having considerable damage size and residual dent) exhibited a progressive dent growth, which was indicated by the dial gauge. The final abrupt failure could be attributed to out-plane tensile fracture of the core on either side of the residual dent, Ref. [18], or to shear fracture in the core layer, Fig. 2(right).

*Face breaking* in the manner of plastic hinge. The indented beams with H130 core having considerable damage size and residual dent exhibited the progressive dent growth but failed at the dent centre, due to the maximum bending moment in the face sheet.

The first two failure modes are characterized by negligible dent growth prior to final failure. A typical load–displacement response for this case is shown in Fig. 5. The load curve is close to linear up to failure, although a reduction in the overall stiffness is observed at the final stage of the curve. This change can be associated with non-linear deformations in the face under a high stress. A typical load–displacement response of a specimen exhibited the dent growth (third and fourth failure modes) is shown in Fig. 6. At a certain moment, the dent growth rate increased abruptly as can be seen in Fig. 6(right). Simultaneously, the overall stiffness decreased, Fig. 6(left), and the overall bending occurred. The overall stiffness was estimated as the tangent to the load curve as shown in Figs. 5(left) and 6(left). As Fig. 7(left) depicts, the drop in stiffness due to local buckling was twice greater that should be associated with the overall bending.

For comparison, a number of virgin specimens and specimens with fabricated sub-interface delamination (introduced as 2-mm height cut in the core) were also tested. The undamaged specimens with WF51 or H60 core failed by the wrinkling mode, and the ones with H130 core—by the face yielding. It appeared, therefore, that the failure mechanism of the sandwich beam remains unchanged (face wrinkling or yielding), when the damage covers a relatively small area (i.e. when the damage length is less than the

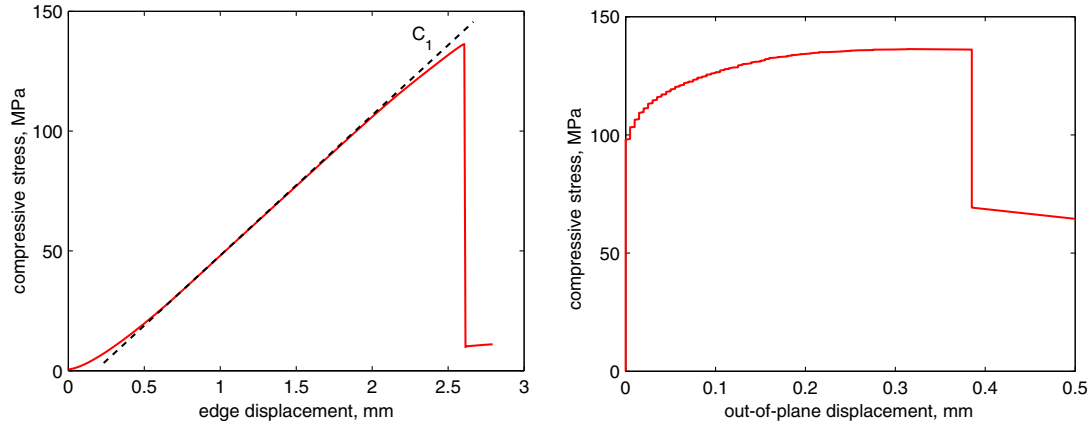


Fig. 5. Results from the edgewise compression tests; a typical load–displacement response (left) and the residual dent growth (right).

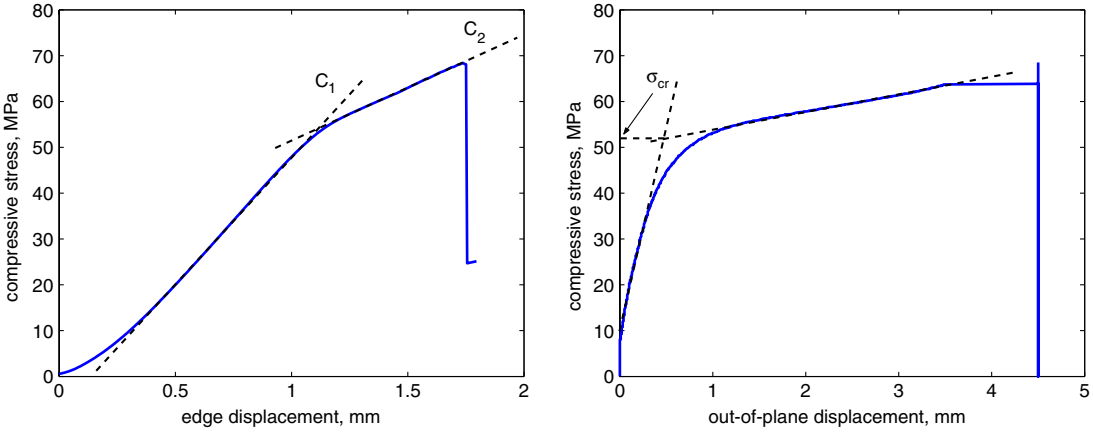


Fig. 6. Results from the edgewise compression tests; a typical load–displacement response (left) and the residual dent growth (right).

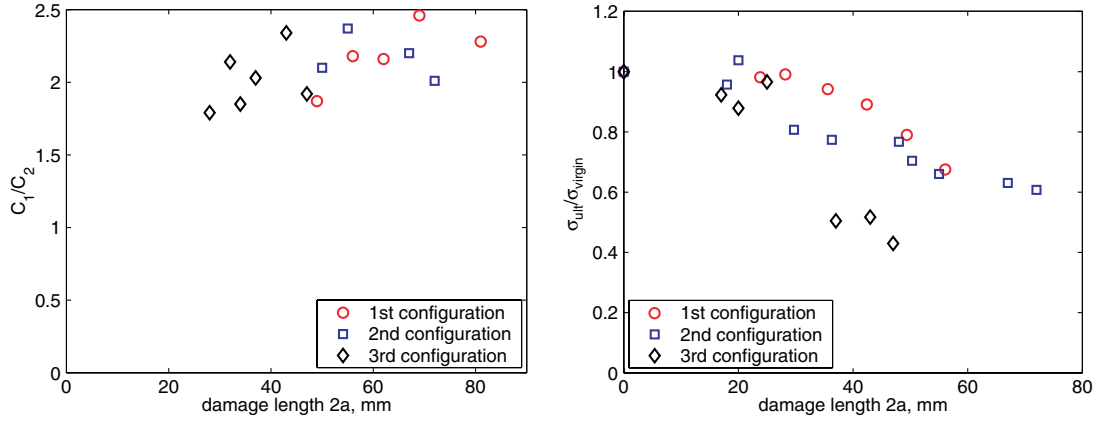


Fig. 7. Ratio of the overall stiffness before ($C_1$) and after ($C_2$) the local buckling (left) and ratio of the ultimate stress of damaged, $\sigma_{ult}$, and virgin, $\sigma_{virgin}$, beams, vs. the damage length (right).

developing wrinkling wavelength). Increasing the damage area caused substantial change in the edgewise compression properties, namely the local buckling in the damaged zone followed by an instantaneous drop in the overall stiffness.

Fig. 7(right) shows the drop in the ultimate (at failure) stress in the face, $\sigma_{ult}$, in comparison with that of the virgin specimens, $\sigma_{virgin}$. As can be seen, the failure by the wrinkling or face yielding does not alter seriously the ultimate stress. Contrary, the failure due to global bending

initiated by the local buckling reduces the ultimate stress up to 40%. However, the ultimate load is obviously dependent on the beam length in the latter case. Also, the formula (1) is valid up to the local buckling or face failure onset.

The results sampled from the edgewise compression tests are summarized in Figs. 8 and 9. The stress associated with the local buckling was determined as the intercept between an extension of the region with steady-state dent magnitude (no dent growth) and a tangent to the region of maximum and constant dent growth, measured by the dial gauge as shown in Fig. 6(right). For large damage, the tests revealed the reduction factor in the critical stresses up to 3. The scatter in the buckling data did not exceed 10%. In Fig. 9(right), a typical dependence is shown of the face dent growth (initial, at the moment of buckling, and ultimate) on the damage length. It is interesting to note that the ratio of the face dent at the moment of buckling to the initial (residual) one was almost constant for each sandwich configuration; respectively, this ratio was 1.17, 1.48, and 1.22 at the average with maximal deviation of 11%.

### 2.5. Uniaxial compression/tension testing of foam cores

The cylindrical specimens with diameter 50 mm were cut from the core blocks in the out-plane direction and then bonded to metallic fixtures of an Instron universal testing machine. The specimens were loaded under 2 mm/min prescribed displacement rate in several steps as shown in Fig. 10(left). First, the specimens were loaded in compression until the foam was fully crushed, see path A–C (region A–B represents the elastic response). Compressive loading was followed by unloading of the specimens and eventual loading in tension (path C–D). This was followed by 10 min relaxation control (path D–E) and secondary compression (path E–F). The more detailed description and analysis of these tests are given in Ref. [20].

For further analytical analysis of the local buckling, the path E–F should be considered in more detail, since it characterizes the core reaction during the inward growth of the face dent. This path contains two distinct linear regions and can roughly be approximated with two moduli, $E'$ and $E''$, as shown in Fig. 10(right). The test data reveals that these moduli are dependent on the strains at the initi-

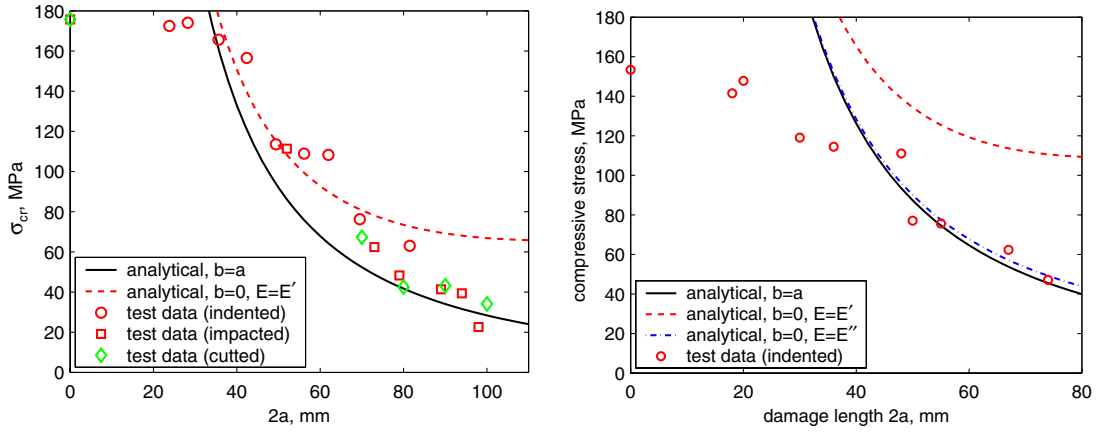


Fig. 8. Euler's stress in the face for first (left) and second (right) sandwich configurations, vs. the damage length.

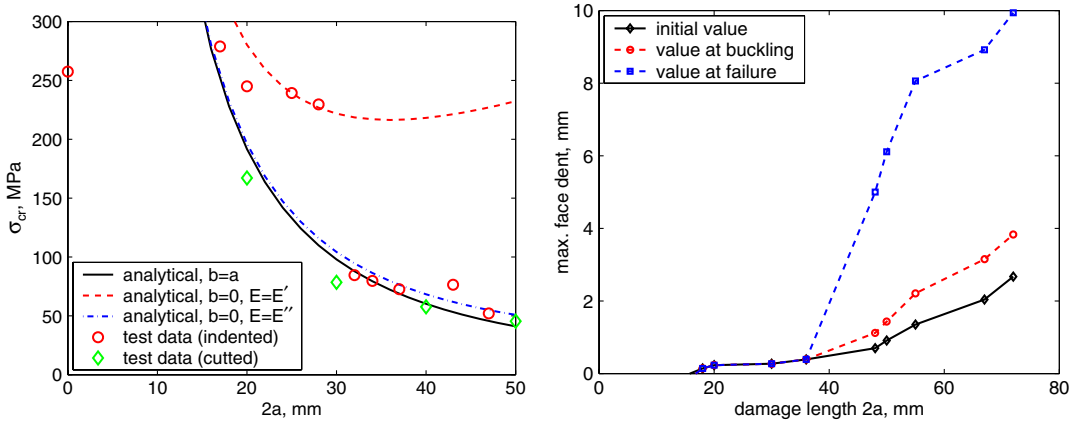


Fig. 9. Euler's stress in the face (left) and the residual dent growth (right) for third sandwich configuration, vs. the damage length.

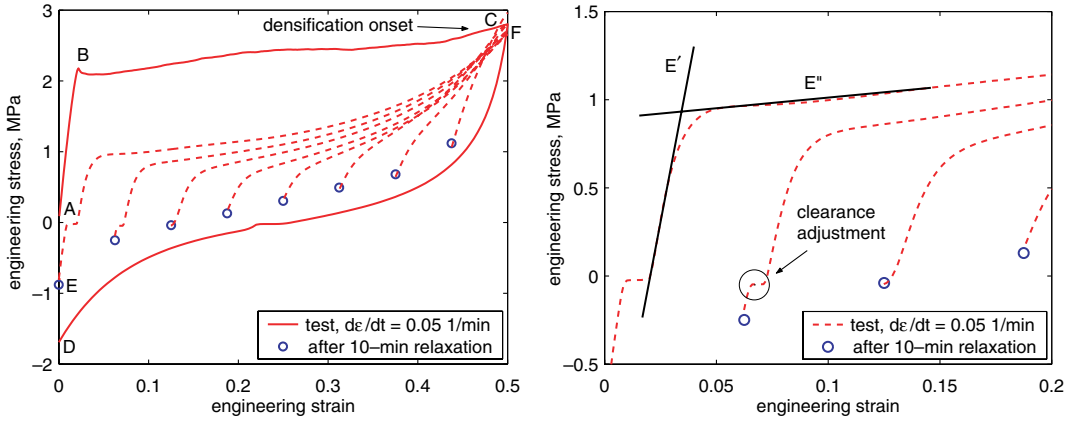


Fig. 10. Stress–strain curves sampled from the uniaxial compression/tension tests on H130 foam specimens; full-scale (left) and zoomed (right).

Table 2
Stiffness of the crushed core under secondary compression

| Configuration | Initial strain $\varepsilon_E$ | | Modulus $E'$, MPa | | | Modulus $E''$, MPa | | |
|---|---|---|---|---|---|---|---|---|
| | 1 | 2 | 1 | 2 | Mean | 1 | 2 | Mean |
| 1 | 0.10 | 0.20 | 8.2 | 7.8 | 8.0 | 0.04 | 0.1 | 0.07 |
| 2 | 0.10 | 0.20 | 20.3 | 15.0 | 17.7 | 0.8 | 1.2 | 1.0 |
| 3 | 0.06 | 0.12 | 63.2 | 46.0 | 54.6 | 2.2 | 3.4 | 2.8 |

ation of the reloading, $\varepsilon_E$, i.e. on the position of point E. This is shown in Table 2, where the moduli are given for two sets of the residual strains $\varepsilon_E$. Considering the ratio between max. residual dent, $w_0^r$, and the damage depth, $d$, in the indented sandwich beams, the residual strains in the crushed core are 0.06–0.16, 0.06–0.14, and 0.06–0.12 for first, second, and third sandwich configurations, respectively. But an accurate calculation of the moduli is beyond the scope of the present paper. Hence, in the following, we use mean values $E'$ and $E''$ taken from Table 2.

## 3. Analytical study

Reasoning from the experimental study, the present analytical approach is focused on the local buckling in the face expressed in an unstable dent growth. The wrinkling failure and yielding fracture of the face laminate (typical for small damage lengths) are not discussed below.

### 3.1. Physical modelling

The geometry of the model is shown in Fig. 4, where the face sheet in the damage area and its geometrical parameters are represented. Only bending is considered, and the interface shear stresses are neglected. Assuming also that $h_f \ll 2a$, the physical model can be composed as shown in Fig. 11, i.e. as simply supported and elastically clamped beam of unit width. The elastic clamp is used to model the reacting moment from the undamaged part of the sandwich structure. The beam is subject to an edgewise compression by the "dead" end force $\sigma h_f$ (per unit width of the beam), where $\sigma$ is the compressive stress in the face. The critical (in the Euler's sense) value of $\sigma$ is to be determined.

Two variants of this general model are considered below; $b = a$ and $b = 0$. The first variant, Fig. 11(a), represents the case when the core damage contains a cavity eliminating the core support over all damaged zone. The second variant, Fig. 11(b), represents the case of continuous support from the crushed core. In both variants, the modelling approach assumes no influence of the residual dent in the face on the buckling behaviour. This assumption may be adopted, since the experimental study shows that (1) the buckling shape coincides with the shape of the residual dent, and (2) the residual dent is less than the face thickness, and no considerable dent growth occurs prior to the buckling onset.

### 3.2. Mathematical modelling and 'exact' solution for the case $b = a$

The mathematical model is composed using the thin plate Kirchhoff theory. The governing equation of the cylindrical bending written for the midplane rotation $\theta_f$ is

$$D_f \theta_f''(x) + \sigma h_f \theta_f(x) = 0, \tag{2}$$

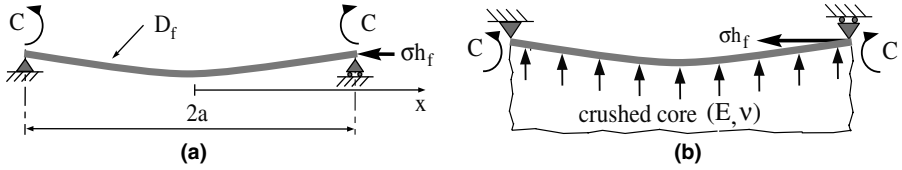


Fig. 11. The modelling approach for the case of (a) face-crushed core debond and (b) perfect interfacial bonding. The buckled face sheet is shown schematically.

where for the plane strain formulation $D_f = E_f h_f^3/12(1-\nu_f^2)$. The elastic clamp condition is

$$x = \pm a: \quad D_f \theta_f'(x) = \mp C\theta_f(x), \tag{3}$$

where $C$ is the rotational stiffness, which is determined below in Section 3.6.

Eq. (2) has a non-trivial solution of the following view:

$$\theta_f(x) = A \cdot \sin(\lambda x), \tag{4}$$

where, according to Eq. (3), the parameter $\lambda$ is the root of equation

$$\tan(a\lambda) = -a\lambda/k, \quad \text{where } k(a) = aC/D_f, \tag{5}$$

at that the least non-zero root corresponds to the Euler's stress at the first buckling mode. This stress is determined substituting Eq. (4) into Eq. (2) as

$$\sigma_{cr} = D_f \lambda^2 / h_f. \tag{6}$$

Figs. 8 and 9 show a comparison of analytical results obtained using Eq. (6) with the experimental data. As can be seen, the solution (6) provides quite correct estimation of the Euler's stress in the face at large damage lengths. The exception are several sets of specimens having moderate damage length and no cavity; this case is investigated further. The experimental data for specimens with fabricated debonds is in better agreement with the analytical solution than for the indented or impacted specimens. This fact can obviously be explained as by some reduction in the face stiffness due to impact or indentation, as well as by some influence from the crushed core. These effects are eliminated in the specimens with fabricated debond, in which the face stiffness is virgin, and the damage length is equivalent to the cavity length.

The use of Eq. (6) also provides good agreement with the experimental results given in Ref. [21] for debonds implanted using non-stick teflon inserts. Though, the referred study contains only 2–3 values of the critical stresses for each sandwich configuration, at that only 1–2 points can be attributed to the range of elastic deformations in the face sheet.

### 3.3. Mathematical modelling and 'exact' solution for the case $b = 0$

If no cavity is formed after unloading ($b = 0$), Fig. 11(b), the local buckling behaviour is somehow affected by the damaged core. This case can be investigated using the governing equation

$$D_f \theta_f'''(x) + \sigma h_f \theta_f'(x) = \sigma_{if}(x), \tag{7}$$

where item $\sigma_{if}$ represents a supporting effect of the crushed core. This function can approximately be obtained considering an elastic half-plane with the boundary deformed according to (4). The half-plane behaviour is described by the static Lamé equations for isotropic elastic continuum

$$\begin{aligned} 2(1-\nu)\frac{\partial^2 w}{\partial z^2} + (1-2\nu)\frac{\partial^2 w}{\partial x^2} + \frac{\partial^2 u}{\partial x \partial z} = 0, \\ 2(1-\nu)\frac{\partial^2 u}{\partial x^2} + (1-2\nu)\frac{\partial^2 u}{\partial z^2} + \frac{\partial^2 w}{\partial x \partial z} = 0, \end{aligned} \tag{8}$$

where $\nu$ is the Poisson's ratio of the crushed core. The unknown functions $u \equiv u(x,z)$ and $w \equiv w(x,z)$ are displacements in the longitudinal, $x$, and transversal, $z$, directions, respectively. The solution of Eq. (8) can be represented as

$$\begin{aligned} u &= \left(e^{-\lambda z}(K_1 + K_2\lambda z) + e^{\lambda z}(K_3 + K_4\lambda z)\right)\sin(\lambda x), \\ w &= \left(e^{-\lambda z}(C_1 + C_2\lambda z) + e^{\lambda z}(C_3 + C_4\lambda z)\right)\cos(\lambda x). \end{aligned} \tag{9}$$

The boundary conditions are

$$\begin{aligned} &z = 0: \quad u = 0, \quad w = A\cos(\lambda x), \\ &z \to \infty: \quad u \to 0, \quad w \to 0, \end{aligned} \tag{10}$$

that yields

$$C_3 = C_4 = K_1 = K_3 = K_4 = 0, \quad K_1 = A. \tag{11}$$

The other two constants are determined substituting Eq. (9) into Eq. (8) as

$$C_2 = -K_2 = A/(3-4\nu). \tag{12}$$

Finally, the normal interface stress is determined as (for the plane strain state)

$$\sigma_{if} = \frac{E(1-\nu)}{(1+\nu)(1-2\nu)}\left(\frac{\partial w}{\partial z} + \frac{\nu}{1-\nu}\frac{\partial u}{\partial x}\right) = -E_1 A\lambda\cos(\lambda x), \tag{13}$$

where $E$ is assumed to be the Young's modulus of the crushed core in the direction of the cells compacting during the foam core crushing. This assumption is conservative, since the in-plane (perpendicular to the direction of the cells compacting) modulaes of the crushed WF- and H-grade cores are almost the same as those of undamaged cores [19]. The factor $E_1$ is

$$E_1 = \frac{2E}{(1+\nu)(3-\nu)} \quad \text{or} \quad E_1 = \frac{2E(1-\nu)}{(1+\nu)(3-4\nu)}$$

for the plane stress or strain states, respectively. The Euler's stress at the first buckling mode is determined substituting Eqs. (4) and (13) into Eq. (7) as

$$\sigma_{cr} = D_f \lambda^2 / h_f + E_1 / \lambda h_f, \tag{14}$$

where $\lambda$ is as before the least non-zero root of Eq. (5).

The results through Eq. (14) are presented in Figs. 8 and 9. When calculating the factor $E_1$, we used mean values of the modulus $E'$ from Table 2 and $\nu = 0.5$. In general, Eq. (14) predicts the Euler's stress with good accuracy for the beams with moderate damage lengths and without cavities. This is because these specimens had minor inward growth of the residual dent up to the moment of buckling; thus, the core reaction followed the relatively large modulus $E'$, see Section 2.5. In the beams having large damage lengths (i.e. $2a > 28$ mm for third sandwich configuration), a considerable residual dent growth was provoked, as

shown in Fig. 9(right). This caused a noticeable reduction from $E'$ to $E''$ in the core support, as shown in Table 2 (for first configuration in 25 times) and, as a result, drastic drop in the local buckling stress. This effect is depicted in Figs. 8 and 9, where the results by Eq. (14) using $E''$ are shown for second and third sandwich configurations.

It should also be pointed out that for investigated sandwich configurations, at small and moderate damage lengths, the proportional limit of the face material is reached well before the elastic buckling occurs. This fact is indicated by the load curves sampled from the edgewise compression tests, Section 2.4. The results by Eq. (14) can thus be improved accounting for the secant modulus of the face material but this is beyond the scope of this study.

### 3.4. Limit solution for the case of large damage in the core

It is obvious, the undamaged part of the structure has no influence on the buckling stress after the damage length exceeds a certain limit. This limit can be calculated taking derivation of Eq. (14) with respect to $\lambda$. This gives

$$\lambda^* = 1/x_n\sqrt[3]{2}, \quad x_n = \sqrt[3]{D_f/E_1}, \tag{15}$$

where $E_1$ is the reduced modulus from the second part of the path E–F, Fig. 10. Combination of Eqs. (15) and (5) then provides the damage length $2a_0$, at which the face becomes wrinkle as an infinite beam supported by an elastic half-plane with the properties of crushed core. The Euler's stress for this model is determined substituting Eq. (15) into Eq. (14) as

$$\sigma_{cr} = \frac{3}{\sqrt[3]{4}}\frac{x_n}{h_f}E_1, \tag{16}$$

that gives the lower limit (threshold level) in the case of the local damage in the core. The results by Eq. (16), as well as by Eqs. (5) and (15) are presented in Table 3. It is seen that for the investigated sandwich configurations the damage length $2a_0$ cannot be exceeded without a serious damage in the face. It should be pointed out that Eq. (16) is similar to the solutions obtained for the uni-directional face wrinkling in undamaged sandwich structures, Ref. [2].

Table 3
Threshold parameters of the local buckling (analytical estimation)

| Configuration | Modulus $E''$, MPa | $\sigma_{cr}$ by Eq. (16), MPa | $2a_0$, mm |
|---|---|---|---|
| 1 | 0.07 | 2.8 | 629 |
| 2 | 1.00 | 16.1 | 249 |
| 3 | 2.80 | 29.9 | 110 |

### 3.5. Approximate solution

The Ritz method can be utilized for an approximate study of the problems, which are solved above in exact formulations. For this, the midplane rotation of the buckled face is taken in the following view:

$$\theta_f(x) = \pi\sin(\pi x/2a) + k\sin(\pi x/a), \tag{17}$$

which satisfies the boundary condition (3). The total energy of the model is

$$\Pi = \int_0^a \left(D\theta_f'^2 - \sigma h_f\theta_f^2 + k_z w_f^2\right)\mathrm{d}x + k\theta_f^2(a) = 0. \tag{18}$$

Here, the parameter $k_z$ is the elastic foundation modulus, which represents the supporting effect of the crushed core. This modulus can approximately be calculated as, Ref. [2],

$$k_z = 0.282E\sqrt[3]{E/D_f}, \quad \bar{k}_z = \frac{k_z}{D_f}\left(\frac{a}{\pi}\right)^4. \tag{19}$$

Substituting (17) into the energy functional (18) gives the following solution for the Euler's stress in the face:

$$\sigma_{cr} = \frac{\pi^2 D_f}{a^2 h_f}\widetilde{f}(k_1),$$
$$\widetilde{f}(k) = \frac{3\pi^2/4 + 10k + 3k^2 + \bar{k}_z(12\pi^2 + 64k + 9k^2)}{3\pi^2 + 16k + 3k^2}. \tag{20}$$

For comparison, Eqs. (14) and (16) are suitable to be rewritten as

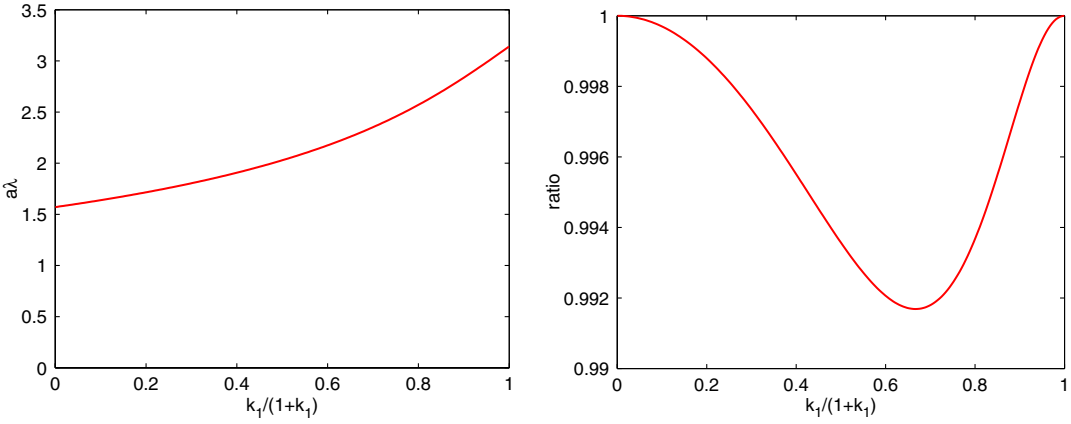


Fig. 12. Roots of Eq. (5) (left) and ratio $\bar{f}(k)/\widetilde{f}(k)$ (right) as functions of restraining parameter $k$. No influence of the crushed core is assumed ($k_z = 0$).

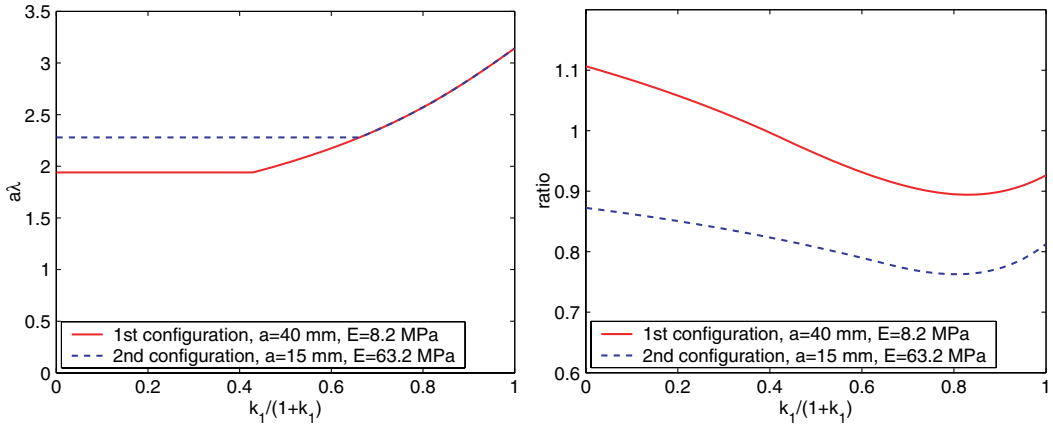


Fig. 13. Roots of Eq. (5) (left) and ratio $\bar{f}(k)/\tilde{f}(k)$ (right). The supporting effect of the crushed core is accounted for.

$$\sigma_{cr} = \frac{\pi^2 D_f}{a^2 h_f}\bar{f}(k),$$
$$\bar{f}(k) = \begin{cases} (a\lambda/\pi)^2(1 + E_1/\lambda^3 D_f), & \text{if } \lambda \geqslant \lambda^*, \\ (a/\pi x_n)^2(3/\sqrt[3]{4}), & \text{if } \lambda \leqslant \lambda^*. \end{cases} \quad (21)$$

Ratios $\bar{f}(k)/\tilde{f}(k)$ are presented in Figs. 12 and 13. Fig. 12 shows that at $k_z = 0$ the error of the approximate solution (20) is negligibly small (<1%). Thus, this closed form formula can be employed instead of the implicit one (6). Fig. 13 shows more poor agreement (within 20%) between exact and approximate solutions at $k_z \neq 0$. Obviously, this relatively large discrepancy can be explained by the use of rough estimation (19) which was derived from a particular problem of local loading of an infinite beam resting on an elastic half-plane that models a very thick core, Ref. [22].

### 3.6. Calculation of the rotational stiffness C

The preceding solutions require the rotational stiffness $C$ introduced in Eq. (3). This stiffness can approximately be determined considering the bending of an infinite face of unit width bonded to an elastic half-plane and loaded by an axial stress $\sigma$ and a line bending moment $M$ as shown in Fig. 14(a). Denoting the Dirac delta-function as $\delta$, the governing equation for the face deflection $w_f$ is given by the thin plate Kirchhoff theory as

$$D_f w_f''''(x) + \sigma h_f w_f''(x) = -M\delta'(x) - \sigma_{if}(x), \quad 0 \leqslant x \leqslant \infty. \quad (22)$$

Applying further the sine Fourier transformation to Eq. (22), we have

$$D_f \omega^4 w_f^F(\omega) - \sigma h_f \omega^2 w_f^F(\omega) = M\omega - \sigma_{if}^F(\omega). \quad (23)$$

The image of the face rotation $\theta_f$ is obtained as

$$\theta_f^F(\omega) = \omega w_f^F(\omega). \quad (24)$$

The image of the core reaction, $\sigma_{if}^F$, is determined through the Lamé equations assuming zero longitudinal displacement and given deflection, $w_f$, of the face. The Fourier-transformed system (8) produces the following relation between the images of the face deflection and normal stress at the interface [23]:

$$\sigma_{if}^F(\omega) = E_1 \omega w_f^F(\omega), \quad (25)$$

where the parameter $E_1$ has the same view as in Eq. (13) but assumes the use of the Young's modulus, $E_c$, and Poisson's ratio, $\nu_c$, of the virgin core.

The closed-form solution for the original of the face rotation is obtained substituting Eq. (25) into Eq. (23), deriving $w_f^F$ and applying the inverse cosine Fourier transformation to Eq. (24). The solution for the max. rotation (under the bending moment) reads

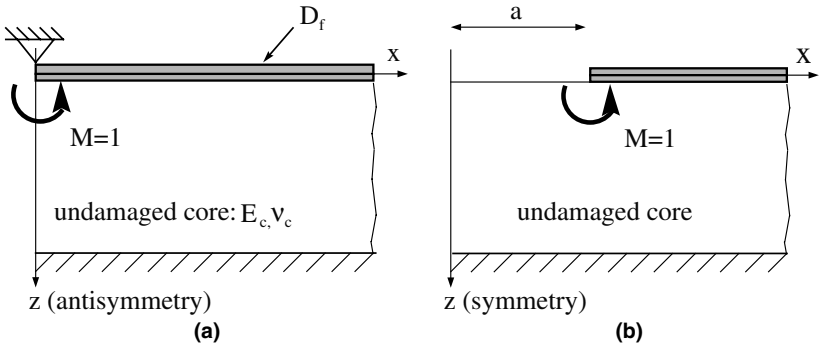


Fig. 14. Geometry and load cases in the analytical (a) and FE (b) modelling.

$$\theta_f = \gamma M \int_0^\infty \frac{\bar{\omega}\,d\bar{\omega}}{\bar{\omega}^3 - \sigma\eta\bar{\omega} + 1}, \tag{26}$$

where $\bar{\omega} = \omega x_n$ is the dimensionless variable of the Fourier transformation, and

$$\gamma = 2/\pi E_1 x_n^2 \approx 4.0 h_f^{-2}(E_c E_f^2)^{-1/3},$$
$$\eta = x_n^2 h_f / D_f \approx 3.3(E_c^2 E_f)^{-1/3}.$$

The rotational stiffness is calculated as the inverse value of the rotation under the unit bending moment. For the simplest case of zero axial stress $\sigma$, the improper integral in Eq. (26) can be derived analytically, and we have

$$C = 0.75\sqrt{3}E_1^{1/3}D_f^{2/3} \approx 0.2 h_f^2 (E_c E_f^2)^{1/3}. \tag{27}$$

The solution (27) was calibrated using the FE package *CosmosM 2000*. A sketch of a two-dimensional FE model is shown in Fig. 14(b). Since the debond was situated symmetrically, only half of a sandwich beam was considered. The model was meshed using 2-node beam elements (BEAM2D) for the face and 4-node shell elements (SHELL4) for the core. The face was composed of one element through the thickness and 50 elements along the face. Twenty elements were used through the thickness of the core. The mesh was refined towards the point of application of the unit bending moment. Results of the linear-elastic FE analysis were used in the preceding analytical calculations; the rotational stiffness was taken of 2.56, 2.21 and 1.21 kN for first, second and third configurations, respectively.

The results of the FE analysis are shown in Fig. 15(left), which depicts the effect of the core thickness on the rotational stiffness of the FE model normalized to the value obtained analytically using Eq. (27). For moderate and large core thickness, it is seen that the analytical solution gives stable deviation in 35% for all sandwich configurations. Thus, a correction factor of 0.7 can be used to fit Eq. (27) without the FE analysis. Fig. 15(right) demonstrates also the effect of accuracy in determination of the rotational stiffness $C$ on the Euler's stress given by Eq. (6). The graph indicates that this effect is small for relatively compliant faces (third configuration), while rigid faces (first and second configurations) exert stronger dependence.

The presented FE study does not account for in-plane compression of the face. However, the particular analysis using Eq. (26) shows that this effect reduces the rotational stiffness not much. This is proved for relatively low compressive stresses relating to the local buckling in the specimens of the investigated configurations. Also, the solution can be improved accounting for inelastic compressive response of the face material, as well as accounting for finite thickness of the core. The later case has been investigated in study [12], though it was seen from Fig. 15(left) that for the case of relatively thick and soft core its thickness was of small importance.

## 4. Conclusions

The edgewise compression response of sandwich beams with indent- or impact-induced damage was experimentally and analytically investigated in this paper. The particular focus was posed on the stability of the face sheet within the damaged zone. The main results can be outlined as the following:

- The experimental study revealed that a typical damage consists of sub-interface zone of crushed core and residual dent in the face sheet. Almost no delamination was observed in the face. For one sandwich configuration subject to impact loading, the core damage contained also a relatively large cavity; this effect reduced considerably the residual face dent.
- Under edgewise compression, the specimens with relatively small damage failed, depending on a configuration, by abrupt wrinkling or yielding (compressive fracture) of the face. These failure modes coincided with ones for undamaged specimens of the same sandwich configurations. When the damage length exceeded a certain size, the failure mechanism changed suddenly to local buckling. The local buckling occurred in the damage zone and was provoked by the residual dent in the face. This failure mode

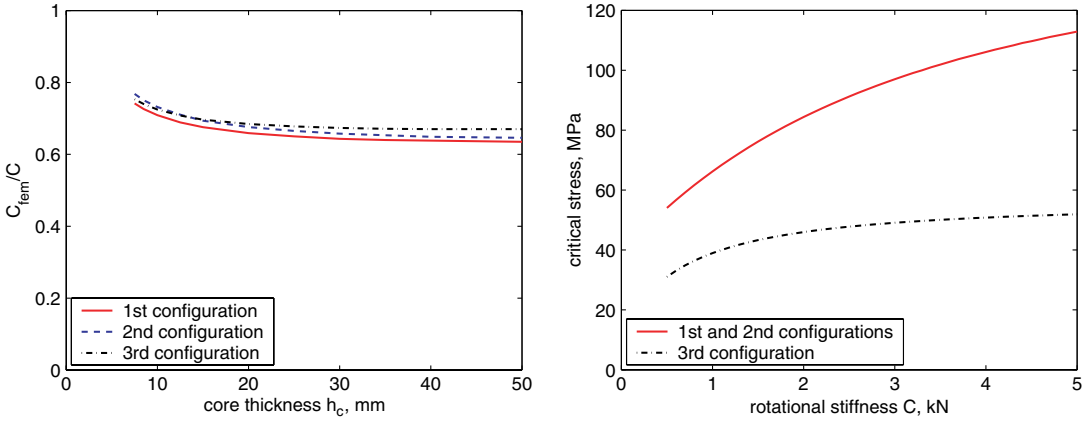


Fig. 15. FE-verification of Eq. (27) (left) and influence of the rotational stiffness $C$ on the Euler's stress by Eq. (6) at $2a = 25$ mm (right).

caused a substantial reduction in the compression load capacity and overall stiffness. For moderate damage lengths and small residual dents, a strong supporting effect of the crushed core was revealed.

• Two analytical solutions predicting the Euler's stress are presented. The first solution assumes no influence of the crushed core on the face buckling and thus gives conservative estimation of the Euler's load. The second, more refined solution, assumes perfect bonding between the face and the crushed core and thus yields the upper limit of the Euler's load. For investigated sandwich configurations, it is found that taking into account the supporting effect of the crushed core rises considerably the Euler's load for the face. The proposed solutions demonstrate good agreement with experimental data. As believed by authors, these solutions can also be utilized for the strength assessment of the sandwich beams with honeycomb or corrugated cores.

## Acknowledgements

Vitaly Koissin wishes to thank the Vera Sagers Stiftelse (Stockholm) for financial support. Some test specimens were kindly supplied by Dr. Per Wennhage (Royal Institute of Technology, Sweden). Authors would also like to thank Mr. Bo Magnusson (ibid) for assistance with experiments.

## References

[1] Mamalis AG et al. On the crushing response of composite sandwich panels subjected to edgewise compression: experimental. Compos Struct 2005;71(2):246–57.
[2] Zenkert D. An introduction to sandwich construction. London: Chameleon Press Ltd; 1995.
[3] Thomson RS, Mouritz AP. Skin wrinkling of impact damaged sandwich composite. J Sandwich Struct Mater 1999;1(4):299–322.
[4] Olsson R. Methodology for predicting the residual strength of impacted sandwich panels. Technical report FFA TN 1997-09. Stockholm: The Aeronautical Institute of Sweden (FFA); 1997.
[5] Kim WC, Miller TC, Dharan CKH. Strength of composite sandwich panels containing debonds. Int J Solids Struct 1993;30(2):211–23.
[6] Vizzini AJ, Lagace PA. The buckling of a delaminated sublaminate on an elastic foundation. J Compos Mater 2004;63(1):1–9.
[7] Niu K, Talreja R. Buckling of a thin face layer on Winkler foundation with debonds. J Sandwich Struct Mater 1999;1(4):259–78.
[8] Avery JL, Sankar BV. Compressive failure of sandwich beams with debonded face-sheets. J Compos Mater 2000;34(14):1176–99.
[9] Rzayev G. Local buckling around an interfacial crack in a viscoelastic sandwich plate. J Mech Comp Mater 2002;38(3):233–42.
[10] Hetényi MI. Beams on elastic foundation. Ann Arbor: University of Michigan Press; 1946.
[11] Wadsworth DJ, Horrigan DPW, Moltschaniwskyj G. Facesheet wrinkling in honeycomb sandwich structure containing sub-interface damage. In: Proc 6th Int Conf on Sandwich Structures (ICSS-6), Fort Lauderdale, USA; 2003. p. 190–201.
[12] Skvortsov V, Koissin V, Shipsha A. Stability of the face layer of sandwich structures with a local interlaminar damage. J Mech Comp Mater 2002;38(6):515–24.
[13] Shipsha A, Hallström S, Zenkert D. Failure mechanisms and modelling of impact damage in sandwich beams—A 2D approach: Part I—experimental investigation. J Sandwich Struct Mater 2003;5(1):7–32.
[14] Shipsha A, Hallström S, Zenkert D. Failure mechanisms and modelling of impact damage in sandwich beams—A 2D approach: Part II—analysis and modelling. J Sandwich Struct Mater 2003;5(1):33–52.
[15] Koissin V. The local strength of foam cored sandwich structures. PhD thesis, Department of Strength of Materials, State Marine Technical University, St.-Petersburg, Russia; 2004 [in Russian].
[16] ROHACELL. Technical Manual. Darmstadt: Röhm GmbH; 1987.
[17] DIVINYCELL. Technical Manual H-Grade. Laholm: Divinycell Int. AB; 1995.
[18] Shipsha A. Edgewise compression of sandwich panels with impact damage. In: Proc 6th Int Conf on Sandwich Structures (ICSS-6), Fort Lauderdale, USA; 2003. p. 154–62.
[19] Koissin V, Shipsha A. Mechanical properties of pre-compressed and undamaged DIVINYCELL H-grade foam core. Report C2001–5, Kungliga Tekniska Högskolan; 2001.
[20] Koissin V, Shipsha A. Deformation of foam cores in uniaxial compression–tension cycle. In: Proc 7th Int Conf on Sandwich Structures (ICSS-7), Ålborg, Denmark; 2005. p. 885–94.
[21] Vadakke V, Carlsson LA. Experimental investigation of compression failure of sandwich specimens with face/core debond. Compos, Part B 2004;36(6–8):583–90.
[22] Biot MA. Bending of an infinite plate on an elastic foundation. J Appl Mech 1937;4(1):A1–7.
[23] Skvortsov VR. Exact analysis of sandwich plates bending based on elasticity theory and the technique of integral transformations. In: Proc 5th Int Conf on Mechanics of Sandwich Structures, Zurich; 2000. p. 129–40.